Fluid mechanics of Windkessel effect

As Published: https://doi.org/10.1007/s11517-017-1775-y

Publisher: Springer Berlin Heidelberg

Noname manuscript No.
(will be inserted by the editor)

Fluid Mechanics of Windkessel Effect

C. C. Mei · J. Zhang · H.X. Jing

Received: date / Accepted: date

Abstract We describe a mechanistic model of *Windkessel* phenomenon based on the linear dynamics of fluid-structure interactions. The phenomenon has its origin in an old-fashioned fire-fighting equipment where an air chamber serves to transform the intermittent influx from a pump to a more steady stream out of the hose. A similar mechanism exists in the cardiovascular system where blood injected intermittantly from the heart becomes rather smooth after passing through an elastic aorta. In existing haeodynamics literature this mechanism is explained on the basis of electric circuit analogy with empirical impedances. We present a mechanistic theory based on the principles of fluid/structure interactions. Using a simple one-dimensional model, wave motion in the elastic aorta is coupled to the viscous flow in the rigid peripheral artery. Explicit formulas are derived that exhibit the role of material properties such as the blood density, viscosity, wall elasticity, radii and lengths of the vessels. The current two-element model in haemodynamics is shown to be the limit of short aorta and low injection frequency and the impedance coefficients are derived theoretically. Numerical results for different aorta lengths and radii are discussed to demonstrate their effects on the time variations of blood pressure, wall shear stress and discharge.

Chiang C. Mei, Department of Civil and Environmental Engineering, Massacheusetts Institute of Technology, Cambridge, MA,02139, USA E-mail: ccmei@mit.edu
Jun Zhang, Department of Civil and Environmental Engineering, Texas A & M University, College Station, TX 77843, USA
Haixiao Jing, Institute of Water Resources and Hydro-electric Engineering, Xi'an University of Technology, Xi'an, 710048, China

Keywords Cardiovascular haemodyamics · Pulsatile flow · Arterial modeling · Windkessel effect · Fluid/structure interactions · Two-element model

1 Introduction

The Windkessel Effect is an important phenomenon in cardiovascular haemodynamics. Windkessel means air chamber in German whose role in old-fashioned fire-engine bears some similarity to the elastic aorta that affects arterial pulses, as explained by the classic work of [1]. Comprehensive review and historical survey of the literature on this and related to phenomenon has been given in [10, 22]. One of the prominant physical features is that while blood enters the aorta from the heart in intermittent spurts, it always flows out of the peripheral arteries and the smaller capillaries downstream as more continuous pulsations. By putting a balloon between a pump and a long rubber tube, experimental simulations of the windkessel effect even show that the outflow can be practically steady(e.g., [13]).

In recent years many haemodynamic problems involving fluid/solid interactions have been modeled by highly computational solution of the equations governing the two coupled phases (e.g., [14, 15]). Existing mathematical descriptions of the windkessel effect have however been dominated by simplifed impedance models familiar in the electric circuit theories. In the simplest two-parameter model [6], the elastic aorta serves only as a reservoir whose volume variation causes a pressure difference between the left ventricle and the peripheral artery. This model resembles the Helmholtz mode in an acoustic cavity where pressure and density change due to the compressibility of air. More complex models involving three or four parameters have been proposed for better matching with experiments [22]. The numerical values of the parameters are determined by fitting predicted velocity and pressure with their measured values from specific experiments. Various techniques for determining these parameters, such as the Pulse Pressure Method (PPM), have been developed [16]. In addition to volume expansion and compaction, the role of wave propagation in the aorta has also been emphasized by several authors [6, 8]. It has been pointed out that occlusions, discontinuities or bifurcations can cause wave reflections in aorta [4, 19, 21]. These effects require the recognition that the aorta is not too short, as implied by the volume expansion and contraction assumption in the classical model [7]. For treating such issues Wave Intensity Analysis was introduced by Parker [11] and has been applied by others[17, 20, 23, 24]. In the Reservoir-Wave Approach, Wang et al. [23] reasoned that pressure changes are due not only to the passage of waves but also to a change in volume of an elastic vessel or to a change in chamber elasticity, as occurs during ventricular contraction and relaxation, Thus the measured pressure should be the sum of a volume-related pressure and a wave-related pressure. A recent review has been given by Tyberg [18].

Many of these studies still rely on the use of empirical impedance parameters such as compliance and resistance. In this article we wish to present a mechanistic theory where only the material properties and the geometric dimensions of the structure are needed. For illustration we consider the simple model shown in Figure 1 where an elastic aorta of mean radius $\widehat{R}$ and length $\widehat{L}$ is connected to the heart at one end and to a rigid peripheral artery of smaller radius R and length L at the other. Blood enters the aorta from the heart at the averaged velocity $U_H(t)$ which is a periodic sequence of isolated pulses and flows out of the peripheral artery to the surrounding environment of known pressure. Based on the theory of fluid/structure interactions, we first investigate the physics. We shall show that for a short aorta the downstream flow out of the artery is pulsatory but continuous as predicted by the classical two-element model. The empirical impedance parameters can however be theoretically derived in terms of the structural properties or the vessel system. We shall also show that for a long compliant section the flow out of the artery can become essentially steady, as is known in the fire-fighting system and demonstrated in laboratory simulations with a balloon [13]. It is hoped that the present work may provide deeper mathematical and mechanistic insight of a problem in arterial haemodynamics.

2 Intermittent Injection from the Heart

We first present a simple model of intermittent influx. Let the area-averaged velocity $U_H(t)$ of blood influx from the left ventricle at $x = 0$ be an infinite series of intermittent pulses which can be expressed as a Fourier series

$$U_H(t) = \sum_{n=-\infty}^{\infty} U_n^H \, e^{i\omega_n t} = \sum_{n=-\infty}^{\infty} U_n^H \, e^{in\pi t/T} > 0, \tag{2.1}$$

where $2T$ is the fundamental period of the pulses, $\omega_1 = \pi/T$ the fundamental frequency, and U_n^H is the amplitude of the n-th harmonic. In particular, U_0^H is the steady (DC) component. For U_H to be real we require that U_{-n}^H equals the complex conjugate of U_n^H, i.e., $U_{-n}^H = (U_n^H)^*$.

Let each pulse be asymmetric and non-zero within a portion of the period. While any realistic injection rate can be modeled by the Fourier series with properly chosen U_n^H, for simplicity we assume it to be of the following form within a typical period of $-T < t < T$:

$$\frac{U_H(t)}{U_{max}} = \begin{cases} \cos\left(\frac{\pi t}{2a}\right), & -a < t < 0, \\ \cos\left(\frac{\pi t}{2b}\right), & 0 < t < b; \\ \quad 0, & -T < t < -a, \quad b < t < T \end{cases} \tag{2.2}$$

where U_{max} is the maximum of U_H. We shall later take $a < b$ so that the rise is steep and the fall is flat. The harmonic amplitudes are readily obtained.

In real form, the influx velocity is

$$U_H(t) = \frac{U_{max}}{2T}\sum_{n=0}^{\infty}\epsilon_n\left\{\frac{(\pi/2a)\cos(n\pi a/T)}{(\pi/2a)^2 - (n\pi/T)^2} + \frac{(\pi/2b)\cos(n\pi b/T)}{(\pi/2b)^2 - (n\pi/T)^2}\right\} \tag{2.3}$$

where ϵ_n is the Jacobi symbol with $\epsilon_0 = 1,\ \epsilon_n = 2, n = 1, 2, 3, ...$ It is easy to see that the series dies out as $1/n^2$ for increasingly large n. Note that there is no singularity at $2a = T/n$ since $\cos\pi/2 = 0$. The time-averaged steady current is

$$U_0^H = \frac{U_{max}}{2T}\left(\frac{1}{\pi/2a} + \frac{1}{\pi/2b}\right) = U_{max}\frac{a+b}{\pi T} \tag{2.4}$$

The time series of the influx $Q_H(t) = \pi\widehat{R}^2 U_H(t)$ is shown for $a = 4T/15,\ b = 8/15T$ in Figure 2.

In the cardiovascular system blood is forced from the ventricle into the elastic aorta, then flows into the peripheral artery. Let us first examine the compliant aorta.

3 Dynamics within the Aorta

Using symbols distinguished by wide hats, we consider an aorta of mean radius $\widehat{R}$ and length $\widehat{L}$. Since the aorta is typically much larger in radius than the peripheral artery, viscosity can be negligible. This is justified by the following estimates of the Womersley number $\alpha = \widehat{R}\sqrt{\omega/\nu}$ which is the ratio of vessel radius to the boundary layer thickness. Take the blood density to be $\rho = 1.05 g/cm^3$, aorta radius $\widehat{R} = O(1.5\ cm)$, kinematic viscosity $\nu = 4 * 10^{-2}\ cm^2/s$. Let the heart rate be 72 beats per minutes (frequency $f = 1.2\ s^{-1}$ or, $\omega = 2\pi * 1.2 = 7.54$ radian/s. The Womersley number $\alpha = 1.5 * \sqrt{7.54/4} * 10 = 20.6$ is rather large. Viscosity is therefore quite negligible except near the wall. In contrast the typical radius of a peripheral artery is $R = O(0.2\ cm)$; the Womersley number is of order unity ($\alpha = 2.93$). Resistance by viscosity must be accounted for.

For the sake of generality, we assume that the aorta length $\widehat{L}$ can be comparable to the typical length of the waves inside. Let $\widehat{U}(x,t)$ denote the area-averaged blood velocity and $\widehat{p}(x,t)$ the difference between the blood pressure inside and the ambient pressure outside the aorta. Neglecting viscosity and nonlinearity, the conservation laws of mass and momentum are

$$\frac{1}{\rho C^2}\frac{\partial \widehat{p}}{\partial t} + \frac{\partial \widehat{U}}{\partial x} = 0, \quad \text{and} \quad \frac{\partial \widehat{U}}{\partial t} + \frac{1}{\rho}\frac{\partial \widehat{p}}{\partial x} = 0, \tag{3.1}$$

throughout the aorta $0 < x < \widehat{L}$. C is the Moens-Korteweg wave speed [2], [12],

$$C = \sqrt{\frac{Eh}{2\rho \widehat{R}}} \tag{3.2}$$

which depends on Young's modulus of elasticity E, the blood density ρ, the thickness h and the radius $\widehat{R}$ of the vessel wall. The two conservation laws can be combined to yield the classical wave equation

$$\frac{1}{C^2}\frac{\partial^2(\widehat{p},\widehat{U})}{\partial t^2} = \frac{\partial^2(\widehat{p},\widehat{U})}{\partial x^2}, \quad 0 < x < \widehat{L}. \tag{3.3}$$

It is known that for human and dogs, $C = 5.8 \sim 8\ m/s$; and peak blood velocity $\widehat{U} \approx 0.5$ m/s [12,3]. Linearity is justifiable since $\widehat{U}/C \ll 1$.

At the ventricular entrance (the heart valve) the boundary condition is

$$\widehat{U}(0,t) = U_H(t) \quad x = 0. \tag{3.4}$$

Matching conditions at the junction ($x = \widehat{L}$) with the peripheral artery will be added later.

Let the unknown aorta pressure be expressed formally as a Fourier series

$$\widehat{p}(x,t) = \sum_{n=-\infty}^{\infty} \widehat{P}_n(x) e^{i\omega_n t}, \tag{3.5}$$

then,

$$\frac{\partial^2 \widehat{P}_n}{\partial x^2} + k_n^2 \widehat{P}_n = 0, \quad \text{where} \quad k_n = \frac{\omega_n}{C}. \tag{3.6}$$

Corresponding to the fundamental mode, $k_1 = \omega_1/C = \pi/CT = 2\pi/\lambda_1$ where $2T$ is the wave period and $\lambda_1 = 2CT$ is the wave length. Formally the solution to (3.6) is

$$\widehat{P}_n(x)e^{i\omega_n t} = \frac{1}{2}\left[(A_n + iB_n)\, e^{-ik_n x} + (A_n - iB_n)\, e^{ik_n x}\right] e^{i\omega_n t} \tag{3.7}$$

which represents the sum of incident and reflected waves.

Let the aorta velocity $\widehat{U}(x,t)$ be of the form,

$$\widehat{U}(x,t) = \sum_{n=-\infty}^{\infty} \widehat{U}_n(x)e^{i\omega_n t} \tag{3.8}$$

Using (3.1),

$$i\omega_n \widehat{U}_n(x) = -\frac{1}{\rho}\frac{\partial \widehat{P}_n}{\partial x} = \frac{k_n}{\rho}\,(A_n \sin k_n x - B_n \cos k_n x)\, e^{i\omega_n t}. \tag{3.9}$$

The unknown coefficients A_n and B_n can be formally solved in terms of the velocity at $x = 0$ and the pressure at $x = \widehat{L}$ by two continuity requirements. Leaving the straightforward details in Appendix A, we cite the result as follows,

$$\widehat{P}_n(x) = \left(P_n(\widehat{L}) + \frac{i\omega_n \rho U_n^H}{k_n}\sin k_n \widehat{L}\right)\frac{\cos k_n x}{\cos k_n \widehat{L}} - \frac{i\omega_n \rho U_n^H}{k_n}\sin k_n x \tag{3.10}$$

which can be used in (3.5) to give

$$\widehat{p}(x,t) = \sum_{-\infty}^{\infty}\left\{\left(P_n(\widehat{L}) + \frac{i\omega_n \rho U_n^H}{k_n}\sin k_n \widehat{L}\right)\frac{\cos k_n x}{\cos k_n \widehat{L}} - \frac{i\omega_n \rho U_n^H}{k_n}\sin k_n x\right\} e^{i\omega_n t} \tag{3.11}$$

Using (3.9) at $x = \widehat{L}$, the aorta velocity $\widehat{U}(\widehat{L},t)$ is finally determined in terms of U_n^H and $P_n(\widehat{L})$,

$$\begin{aligned}\widehat{U}(\widehat{L},t) = U_0^H + \sum_{n\neq 0}\frac{k_n}{i\omega_n \rho}&\left[\left(P_n(\widehat{L}) + \frac{i\omega_n \rho U_n^H}{k_n}\sin k_n \widehat{L}\right)\frac{\sin k_n \widehat{L}}{\cos k_n \widehat{L}}\right.\\ &\left.+\frac{i\omega_n \rho U_n^H}{k_n}\cos k_n \widehat{L}\right] e^{i\omega_n t}.\end{aligned} \tag{3.12}$$

The coefficients $P_n(\widehat{L}),\ n = 0, \pm 1, \pm 2, \ldots$ are yet to be found.

4 Flow in the Peripheral Artery

We model the peripheral artery by a rigid tube of radius R and length L occupying the domain $\widehat{L} < x < \widehat{L}+L$. Accounting for laminar viscosity throughout the tube, the governing equation for the internal velocity $u(r,t)$, which is uniform in x but varies significantly in the radial direction, is

$$\rho\frac{\partial u}{\partial t} = -\frac{\partial p}{\partial x} + \mu\frac{1}{r}\frac{\partial}{\partial r}\left(r\frac{\partial u}{\partial r}\right), \quad 0 < r < R \tag{4.1}$$

The pressure gradient in the straight artery, so far unknown, is uniform in x so that

$$p(x,t) = \sum_{n=-\infty}^{\infty} P_n(\widehat{L})\frac{(\widehat{L}+L-x)}{L}e^{i\omega_n t} \tag{4.2}$$

From here on we shall abbreviate $P_n(\widehat{L}) = \widehat{P}_n(\widehat{L})$ by P_n, unless specified otherwise.

The arterial velocity can be formally expanded as

$$u = \sum_{n=-\infty}^{\infty} u_n(r)e^{i\omega_n t} \tag{4.3}$$

With the boundary conditions that $u(R,t) = 0$ and $\frac{\partial u(0,t)}{\partial r} = 0$, the solution by Womersley [25] for one harmonic $n = 1$ can be generalized to higher harmonics of any n,

$$u_n(r) = -\frac{i}{\mu}\frac{P_n}{L}\frac{R^2}{\alpha_n^2}\left(1 - \frac{J_0(i^{3/2}\alpha_n r/R)}{J_0(i^{3/2}\alpha_n)}\right), \qquad n = 0, \pm1, \pm2, \pm3, ... \tag{4.4}$$

where J_0 denotes Bessel function of order 0, and α_n is the Womersley number of the n-th harmonic which is the ratio of radius to the Stokes layer thickness δ_n of the nth harmonic. For positive integer n,

$$\alpha_n^2 = R^2\frac{\omega_n}{\nu} = \frac{4R^2}{\delta_n^2}, \quad \delta_n = \sqrt{\frac{2\nu}{\omega_n}} \tag{4.5}$$

For negative integer $n = -|n|$, $\omega_n < 0$. We replace α_n by $-|\alpha_n|$. Then $J_0(i^{3/2}\alpha_n)$ becomes $J_0(i^{3/2}i^2|\alpha_n|) = J_0(i^{1/2}|\alpha_n|)$ and $u_{-|n|}$ is the conjugate of $u_{|n|}$ since $i^{9/2} = i^{1/2} = (i^{3/2})^*$.

By integrating (4.1) across the tube,

$$\rho\pi R^2\frac{\partial\langle u\rangle}{\partial t} = \pi R^2\frac{1}{L}\sum_{n=-\infty}^{\infty} P_n\, e^{i\omega_n t} + \mu 2\pi R\left[\frac{\partial u}{\partial r}\right]_R \tag{4.6}$$

where

$$\langle u\rangle = \sum_{n=-\infty}^{\infty} \langle u_n\rangle\, e^{i\omega_n t} = \frac{1}{\pi R^2}\int_0^R u(r)\, 2\pi r dr \tag{4.7}$$

is the area averaged velocity in the artery. From the combination of (4.3) and (4.4), the frictional resistence on the wall is

$$\begin{aligned} 2\pi R\left[\mu\frac{\partial u}{\partial r}\right]_{r=R} &= 2\pi R\mu \sum_{n=-\infty}^{\infty} n e^{i\omega_n t}\frac{\partial u_n(r)}{\partial r}\bigg|_{r=R} \\ &= -2\pi R\sum_{n=-\infty}^{\infty} e^{i\omega_n t}\left\{\frac{P_n}{L}\frac{R^2}{i\alpha_n^2} i^{3/2}\alpha_n \frac{J_0'(i^{3/2}\alpha_n)}{J_0(i^{3/2}\alpha_n)}\right\} \end{aligned} \tag{4.8}$$

It follows from (4.6) that, for each harmonic

$$\langle u_n\rangle = \frac{P_n}{i\omega_n\rho L}\left[1-2\frac{i^{1/2}}{\alpha_n}\frac{J_0'(i^{3/2}\alpha_n)}{J_0(i^{3/2}\alpha_n)}\right] \tag{4.9}$$

We also get the wall stress from (4.4):

$$\tau_w = \mu\left.\frac{\partial u}{\partial r}\right]_R = -\sum_{n=-\infty}^{\infty} e^{i\omega_n t}\left\{\frac{P_n}{L}R^2\frac{i^{1/2}}{\alpha_n}\frac{J_0'(i^{3/2}\alpha_n)}{J_0(i^{3/2}\alpha_n)}\right\}. \tag{4.10}$$

Finally we determine $P_n \equiv P_n(\widehat{L})$ by requiring flux continuity at the junction $x=\widehat{L}$.

$$\pi R^2\langle u\rangle = \pi\widehat{R}^2\widehat{U}(\widehat{L}) \tag{4.11}$$

Using (3.12) and (4.9), we get

$$\begin{aligned} &\pi R^2\frac{P_n}{i\omega_n\rho L}\left[1-2\frac{i^{1/2}}{\alpha_n}\frac{J_0'(i^{3/2}\alpha_n)}{J_0(i^{3/2}\alpha_n)}\right] \\ &= \pi\widehat{R}^2\left\{\frac{k_n}{i\omega_n\rho}\left[\left(P_n+\frac{i\omega_n\rho U_n^H}{k_n}\sin k_n\widehat{L}\right)\frac{\sin k_n\widehat{L}}{\cos k_n\widehat{L}}\right.\right. \\ &\qquad \left.\left.+\frac{i\omega_n\rho U_n^H}{k_n}\cos k_n\widehat{L}\right]\right\} \end{aligned} \tag{4.12}$$

Thus P_n is finally determined in terms of the known U_n^H for all n,

$$P_n = \frac{\frac{\pi\widehat{R}^2}{\cos k_n\widehat{L}}U_n^H}{\frac{\pi R^2}{i\omega_n\rho L}\left[1-2\frac{i^{1/2}}{\alpha_n}\frac{J_0'(i^{3/2}\alpha_n)}{J_0(i^{3/2}\alpha_n)}\right]-\frac{\pi\widehat{R}^2 k_n}{i\omega_n\rho}\frac{\sin k_n\widehat{L}}{\cos k_n\widehat{L}}}. \tag{4.13}$$

With this result the arterial velocity and wall shear stress can be obtained in terms of the influx velocity from the ventricle. In particular (4.9) gives the harmonic amplitude $\langle u_n \rangle$ of the artery velocity

$$\langle u_n \rangle = \frac{P_n}{i\omega_n \rho L}\left[1{-}2\frac{i^{1/2}}{\alpha_n}\frac{J_0'(i^{3/2}\alpha_n)}{J_0(i^{3/2}\alpha_n)}\right] = \frac{\frac{\widehat{R}^2/R^2}{\cos k_n \widehat{L}} U_n^H}{1 - \frac{(\widehat{R}^2/R^2)k_n L}{\left[1-2\frac{i^{1/2}}{\alpha_n}\frac{J_0'(i^{3/2}\alpha_n)}{J_0(i^{3/2}\alpha_n)}\right]}\frac{\sin k_n \widehat{L}}{\cos k_n \widehat{L}}}$$

$$= \frac{U_n^H}{\frac{R^2}{\widehat{R}^2}\cos k_n \widehat{L} - \frac{k_n L \sin k_n \widehat{L}}{\left[1-2\frac{i^{1/2}}{\alpha_n}\frac{J_0'(i^{3/2}\alpha_n)}{J_0(i^{3/2}\alpha_n)}\right]}} \qquad (4.14)$$

after using (4.13) in (4.9). The artery velocity $\langle u \rangle$ follows from (4.7).

We stress that the preceding results hold for all integrals $n = 0, 1, 2, \ldots$. The special case of $n = 0$ can either be obtained by taking the limit of vanishing argument of J_0 in (4.4), to get

$$u_0(r) = \frac{P_0}{4\mu L}(R^2 - r^2) \qquad (4.15)$$

or derived directly from the momentum equation for the zeroth harmonic

$$0 = \frac{P_0}{L} + \mu \frac{1}{r}\frac{\partial}{\partial r}\left(r\frac{\partial u_0}{\partial r}\right). \qquad (4.16)$$

and the boundary conditions

$$u_0 = 0, \quad r = R; \qquad \frac{\partial u_0}{\partial r} = 0, \quad r = 0. \qquad (4.17)$$

By taking the cross-sectional average

$$\langle u_0 \rangle = \frac{1}{\pi R^2}\int_0^R 2\pi r u_0 dr = \frac{P_0 R^2}{8\mu L} \qquad (4.18)$$

one finds the relation

$$P_0 = \frac{8\mu L}{R^2}\langle u_0 \rangle. \qquad (4.19)$$

As a check, we take $n = 0$ in (4.13) to find,

$$P_0 = 8\left(\rho \frac{L\nu}{R^2} U_0^H\right)\frac{\widehat{R}^2}{R^2} \qquad (4.20)$$

since $\alpha_0 = 0$. This result can be used in (4.19) to get

$$\langle u_0 \rangle = \frac{R^2}{8\mu L} 8\left(\rho\frac{L\nu}{R^2}U_0^H\right)\frac{\widehat{R}^2}{R^2} = U_0^H \frac{\widehat{R}^2}{R^2} \qquad (4.21)$$

which is of course the steady part of (4.11).

5 Physical Deductions and Limiting Cases

5.1 Effects of artery radius, viscosity and/or frequency

In the denominator of (4.13), the first term

$$F_n = |F_n|e^{i\theta_n} = \frac{1}{i}\left[1-2\frac{i^{1/2}}{\alpha_n}\frac{J_0'(i^{3/2}\alpha_n)}{J_0(i^{3/2}\alpha_n)}\right] \tag{5.1}$$

represents the effect of viscous resistance in the artery and wave frequency. The exact behavior of F_n is plotted in Figure 3 for a wide range of α_n. For large Womersley's number ($\alpha_n \gg 1$, i.e., low viscosity or high frequency), we get $F_n \to -i$.

For all n, $0 < |F_n| < 1$. Since the n-th term in the Fourier series of $\widehat{p}, p, \widehat{u}$ and $\langle u \rangle$ diminishes with $U_n^H(t)$ as $O(n^{-2})$, only the lowest few modes are numerically dominant. Let us consider the limit of small α_n, i.e., small artery, high viscosity or low frequency, and denote $z = i^{3/2}\alpha_n$ so that

$$2\frac{i^{1/2}}{\alpha_n}\frac{J_0'(i^{3/2}\alpha_n)}{J_0(i^{3/2}\alpha_n)} = -\frac{2J_0'(z)}{zJ_0(z)} \tag{5.2}$$

Since for small z, i.e., small Womersley number,

$$J_0(z) = 1 - \frac{z^2}{4} + \frac{z^4}{2^4(2!)^2} + \cdots, \quad J_0'(z) = -\frac{z}{2} + \frac{z^3}{2^2(2!)^2} + \cdots \tag{5.3}$$

$$\frac{J_0'(z)}{zJ_0(z)} = \frac{-\frac{1}{2} + \frac{z^2}{2^2(2!)^2} + \cdots}{1 - \frac{z^2}{4} + \frac{z^4}{2^4(2!)^2} + \cdots} = F(z^2) = F(-i\alpha_n^2) \tag{5.4}$$

we get

$$\frac{1}{i}\left\{1 - 2\frac{i^{1/2}}{\alpha_n}\frac{J_0'(i^{3/2}\alpha_n)}{J_0(i^{3/2}\alpha_n)}\right\} \approx \frac{\alpha_n^2}{8} = R^2\frac{\omega_n}{8\nu} \tag{5.5}$$

i.e.,

$$F_n \approx \frac{\alpha_n^2}{8} = R^2\frac{\omega_n}{8\nu} \tag{5.6}$$

This approximation is compared with the exact expression in Figure 3, showing good agreement within the range $0 < \alpha_n < 1.5$.

From (4.13) P_n reduces to

$$P_n = \frac{\frac{\pi\widehat{R}^2}{\cos k_n\widehat{L}}U_n^H}{\frac{\pi R^2}{\rho L}\frac{R^2}{8\nu} - \frac{\pi\widehat{R}^2 k_n}{i\omega_n\rho}\frac{\sin k_n\widehat{L}}{\cos k_n\widehat{L}}}, \quad \alpha_n \ll 1. \tag{5.7}$$

Note that the viscous resistance term in P_n no longer depends on n, as in the conventional two-element model to be reexamined later.

5.2 Short aorta

Let us next consider the role of elastic deformation of the aorta wall. Again we focus on the first few n in the Fourier series. Consider in particular a short aorta and arbitrary α_n. We let $k_n\widehat{L} \ll 1$ in (5.7), so that $\cos k_n\widehat{L} \to 1$, $\sin k_n\widehat{L} \to k_n\widehat{L}$, and

$$-\frac{\pi\widehat{R}^2 k_n}{i\omega_n\rho}\frac{\sin k_n\widehat{L}}{\cos k_n\widehat{L}} \to i\frac{k_n}{\omega_n}\frac{\pi\widehat{R}^2 k_n\widehat{L}}{\rho} = i\omega_n\frac{\pi\widehat{R}^2\widehat{L}}{\rho C^2} \tag{5.8}$$

It follows that

$$P_n \to \frac{\pi\widehat{R}^2 U_n^H}{\frac{\pi R^2}{i\omega_n\rho L}\left[1-2\frac{i^{1/2}}{\alpha_n}\frac{J_0'(i^{3/2}\alpha_n)}{J_0(i^{3/2}\alpha_n)}\right] + \frac{\pi\widehat{R}^2\widehat{L}}{\rho C^2}i\omega_n}. \tag{5.9}$$

This result can be derived independently as shown in Appendix A. From (5.10) we get

$$\langle u_n\rangle = \frac{U_n^H}{\frac{R^2}{\widehat{R}^2} - \frac{k_n L\, k_n\widehat{L}}{\left[1-2\frac{i^{1/2}}{\alpha_n}\frac{J_0'(i^{3/2}\alpha_n)}{J_0(i^{3/2}\alpha_n)}\right]}} \tag{5.10}$$

In particular, if there is no aorta, $\widehat{L} = 0$, we get

$$\langle u_n\rangle = U_n^H\frac{\widehat{R}^2}{R^2} \tag{5.11}$$

so that

$$\langle u\rangle = \sum_{-\infty}^{\infty}\langle u_n\rangle e^{i\omega_n t} = \frac{\widehat{R}^2}{R^2}\sum_{-\infty}^{\infty}U_n^H e^{i\omega_n t} = \frac{\widehat{R}^2}{R^2}U_H(t). \tag{5.12}$$

Flow in the peripheral artery is just as intermittent as the influx, maintained by the pressure gradient given in(4.2). This intermittency is expected since change to smoother flow is entirely contributed by the compliant aorta.

6 Reduction to the Classical Two-element Model

We shall show in this section that the conventional two-element model is the limit of the wave theory for short aorta and low frequency.

In the two-element model the flow rate is assumed to be affected only by the volume change of the aorta and wall friction in the artery. Using linear approximations for both parts, mass conservation requires

$$Q(t) = \pi\widehat{R}^2 U_H(t) = K\frac{\partial p}{\partial t} + \frac{p}{f} \tag{6.1}$$

where $Q(t)$ denotes the influx rate, K the compliance and f the resistance. For a periodic influx,

$$Q(t) = \sum_{n=-\infty}^{\infty} Q_n e^{i\omega_n t} \quad \text{where} \quad Q_n = \pi \widehat{R}^2 U_n^H \tag{6.2}$$

the blood pressure is

$$p = \sum_{n=-\infty}^{\infty} P_n e^{i\omega_n t}, \quad \text{where} \quad P_0 = fQ_0, \quad P_n = \frac{Q_n}{\frac{1}{f} + i\omega_n K} \tag{6.3}$$

The blood discharge rate in the artery is

$$Q = \frac{p}{f} = \frac{1}{f} \sum_{n=-\infty}^{\infty} P_n e^{i\omega_n t} = \frac{1}{f} \sum_{n=-\infty}^{\infty} \frac{Q_n}{\frac{1}{f} + i\omega_n K} \tag{6.4}$$

For very large K (soft aorta),

$$Q(t) \approx Q_0 = \frac{P_0}{f} \tag{6.5}$$

The flux is dominated by the steady part and is no longer pulsatory.

Returning to our wave theory, if the Womersley number in the peripheral artery is small and the aorta is short, then (4.13) (or (5.7),(5.9)) reduces to

$$P_n = \frac{\pi \widehat{R}^2 U_n^H}{\frac{\pi R^4}{8\rho L \nu} + i\omega_n \frac{\pi \widehat{R}^2 \widehat{L}}{\rho C^2}}, \quad \alpha_n \ll 1, \quad k_n \widehat{L} \ll 1. \tag{6.6}$$

Eq.(6.6) is of the same form as (6.3). The empirical resistance and conductance can be identified to be

$$\frac{1}{f} = \frac{\pi R^4}{8\rho L \nu}, \quad K = \frac{\pi \widehat{R}^2 \widehat{L}}{\rho C^2}. \tag{6.7}$$

Thus the conventional impedance parameters are now theoretically derived and related to the structural properties of the vascular system. In particular the compliance coefficient K can be large when $\widehat{R}$ and whL are sufficiently large and the capacitance C is small. P_n can then be small for all $n \neq 0$ and overwhelmed by the steady part P_0. Consequently $\langle u(t) \rangle \approx \langle u_0 \rangle$; the outward flow can be nearly uniform in time, as in the fire-fighting hose system.

7 Sample Numerical Results

We now present the numerical results calculated from the full theory.

7.1 Inputs

The following inputs are fixed in our first example: $\rho = 1.06(g/cm^3)$, $\nu = 3.3 \times 10^{-2}(cm^2/s)$, $C = 440(cm/s)$, $T = 0.417(s)$, corresponding to the period $2T = 0.834$(s) or heart beat rate of 72/min. We first choose a large aorta with $\widehat{R} = 3.2$ (cm) and small peripheral artery with $R = 0.29$(cm) and $L = 100$ (cm). By setting $a = 4T/15 = 0.11(s)$, $b = 8T/15 = 0.22(s)$ in (2.2), the ratio U_H/U_{max} is plotted in Figure 2. By combining (2.4) with (4.20) we get

$$P_0 = \frac{8\rho L\nu}{R^2}\frac{a+b}{\pi T}\frac{\widehat{R}^2}{R^2}U_{max} \tag{7.1}$$

In order that the mean blood pressure $P_0 \approx 100$ mmHg, we take $U_{max} = 12.6$ cm/s. The influx discharge rate $Q_H(t) = \pi\widehat{R}^2U_H(t)$ is also plotted in Figure 2. With these inputs the artery parameter is $f = 0.95$ $mmHg/cm^3$ according to (6.7).

7.2 Large Aorta of Different Length

We first examine the effect of aorta lengths examine the results for $\widehat{L} = (5, 10, 15)$ cm. From (6.7), the corresponding compliance factors are K =(1.07, 2.09,3.13) $cm^3/mmHg$ respectively. For these three cases, the blood pressure at the junction($x = \widehat{L}$) is displayed in Figure 4. In all cases the blood pressure increases during the systolic phase when the influx velocity is strong, and decreases during the diastolic phase when the influx is weak. However pressure variation is the largest for the shortest aorta(5 cm) and the smallest for the longest aorta.

Figure 5 shows the outflux discharge in the peripheral artery $Q(t) = \langle u(t)\rangle\, \pi R^2$. It is seen that the flux is no longer intermittent and quite continuous with minor fluctuations about the mean. The longer the aorta, the more steady the outflow. This confirms the primary feature of the windkessel effect. Variation of the wall shear stresses τ_w along the peripheral artery is shown in Figure 6. Larger wall shear stress occurs in a shorter aorta. The mean wall shear stress is about -0.14 $mmHg$, or approximately $186 dyn/cm^2$, which is in the range common in human physiology [5].

7.3 Smaller Aorta

Let us consider two smaller aortas of radii $\widehat{R} = (1.5cm, 2cm)$ which are common in humans. For the same length $\widehat{L} = 15cm$, the compliance factors are calculated to be $K = 0.69, 1.22$. Taking $R = 0.25cm$ and $L = 70cm$ for the the peripheral artery, we get $f = 1.2$ from (6.7). To keep the mean pressure P_0 around 100 mmHg, we get from (7.1) that $U_{max} = (46.6\ cm/s, 26.2\ cm/s)$. These velocities correspond to the same maximum influx discharge of $max\ Q_H = 330mL/s$.

The blood pressure at the junction $p(\widehat{L}, t)$, discharge $Q(t)$ and wall shear stress $\tau_w(t)$ in peripheral artery are shown in Figures 7, 8 and 9 respectively. In the smaller aorta, the amplitudes of pressure, discharge and wall shear stress are larger.

8 Concluding remarks

To complement recent interest in the role of waves in windkessel effect, we have described a mechanistic theory of a simple vascular system consisting of an elastic aorta and rigid peripheral artery of much smaller radius. Instead of empirically determined impedances, we assume the material properties and dimensions of the vascular system to be known and treat the fluid-structure interaction based on the linear theory of continuum mechanics. By first allowing a broad range of aorta length and pulsating frequency, we derive analytical expressions of the blood pressure, blood velocity and wall shear stress. In the special limit of short aorta and low frequency, the classical two-element model is recovered and the dependence of the empirical impedances on vessel properties is theoretically derived. Computed pressure and flow velocity for a short aorta show features consistent with typical observations of cardiovascular systems. Results for increasingly long aorta shows the tendency towards steady flow which is in accord with the engineering principle of the fire-fighting equipment that inspired Otto Frank.

Acknowledgement

We thank Dr. Paul McBeth, MD, Foothills Medical Center, University of Calgary, for introducing the topic of Windkessel Effect to CCM.

Appendix A: Details of aorta solution:

Let us first match the velocities at the ventricle, $x = 0$,

$$U_n^H = \widehat{U}_n(0) = -\frac{k_n}{i\omega_n \rho} B_n \tag{A.1}$$

This determines B_n so that

$$\widehat{P}_n(x) = A_n \cos k_n x - \frac{i\omega_n \rho U_n^H}{k_n} \sin k_n x, . \tag{A.2}$$

Clearly, the steady component ($n = 0$) is

$$\widehat{U}_0(0) = U_0^H \tag{A.3}$$

Let the unknown pressure in the peripheral artery be denoted by $p(x, t)$. Because of the assumed rigidity, the pressure gradient in the peripheral artery is constant in x. At the junction $x = \widehat{L}$, $p(\widehat{L}, t)$ may be formally expanded as a Fourier series

$$p(\widehat{L}, t) = \sum_{n=-\infty}^{\infty} P_n(\widehat{L}) e^{i\omega_n t} \tag{A.4}$$

where the coefficients $P_n(\widehat{L})$ are to be found.

We now match the pressure at the junction $x = \widehat{L}$ where the aorta joins the peripheral artery, and get

$$P_n(\widehat{L}) = \widehat{P}_n(\widehat{L}) = A_n \cos k_n \widehat{L} - \frac{i\omega_n \rho U_n^H}{k_n} \sin k_n \widehat{L}, \quad n \neq 0 \tag{A.5}$$

hence

$$A_n = \left(P_n(\widehat{L}) + \frac{i\omega_n \rho U_n^H}{k_n} \sin k_n \widehat{L} \right) \frac{1}{\cos k_n \widehat{L}} \tag{A.6}$$

This leads to (3.10).

Appendix B: Alternative derivation of Eq.(5.9)

Using the dominant harmonic (ω_1, k_1) for scaling, and assuming $k_1 \widehat{L} \ll 1$, the ratio of the two terms in the momentum equation (3.1) is

$$\frac{(1/\rho C^2)\partial \widehat{p}/\partial t}{\partial \widehat{U}/\partial x} = O\left(\frac{\omega_1 C U_{max}}{C^2 U_{max}/\widehat{L}} \right) = O\left(\frac{\omega_1 \widehat{L}}{C} \right) = O(k_1 \widehat{L}) \ll 1 \tag{B.1}$$

Thus $\widehat{U}(t)$ is uniform in x, and the pressure can be related to the radial distention h by a quasi static approximation. Based on extensive experiments with rubber tubes, Olsen and Shapiro [9] found

$$\widehat{p} = \frac{\rho C^2}{2}\left(1 - \frac{S_0^2}{S^2}\right), \tag{B.2}$$

where $S_0 = \pi \widehat{R}^2, \quad S = \pi(\widehat{R} + h)^2$ impedance are the cross-sectional areas before and after distention respectively. For small distention we take the linear approximation,

$$\frac{S_0^2}{S^2} = \frac{1}{(1 + \frac{h}{\widehat{R}})^4} = 1 - 4\frac{h}{\widehat{R}} + \cdots \tag{B.3}$$

so that

$$\widehat{p} = \frac{2\rho C^2 h}{\widehat{R}}; \quad \text{i.e.,} \quad h = \frac{\widehat{p}}{2\rho C^2}\widehat{R}. \tag{B.4}$$

Mass conservation requires that

$$\pi \widehat{R}^2 \widehat{U} - \pi R^2 \langle u \rangle = \widehat{L} 2\pi \widehat{R} \frac{\partial h}{\partial t} = \frac{\pi \widehat{R}^2 \widehat{L}}{\rho C^2} \frac{\partial \widehat{p}}{\partial t} \tag{B.5}$$

It follows by using (3.12) and (4.9) that

$$\begin{aligned} &\pi \widehat{R}^2 \sum_n U_n^H \, e^{i\omega_n t} - \pi R^2 \left\{ \sum_n \frac{P_n}{i\omega_n L} e^{i\omega_n t} \left[-2 \frac{i^{1/2}}{\alpha_n} \frac{J_0'(i^{3/2}\alpha_n)}{J_0(i^{3/2}\alpha_n)} \right] \right\} \\ &= \frac{\pi \widehat{R}^2 \widehat{L}}{\rho C^2} \frac{\partial \widehat{p}}{\partial t} = \frac{\pi \widehat{R}^2 \widehat{L}}{\rho C^2} \sum i\omega_n P_n e^{i\omega_n t} \end{aligned} \tag{B.6}$$

since $\widehat{p}$ is nearly uniform in x and equal to p approximately. This gives (5.9).

References

1. Frank, O., (1899),Grundform des arterielen Pulses. *Zeitschrift. Biologie.* 37, 483-526.
2. Fung, Y. C., (1997), *Biomechanics: Circulation. §. 2.1.* Springer-Verlag.
3. Khir AW, Zambanini,A. Parker , KH. (2004) Local and regional wave speed in the aorta: effects of arterial occlusion *Medical Engineering & Physics,* 26 (2004) 23-29.
4. Khir, A. & Parker, K.H., (2005) Wave intensity in the ascending aorta: effects of arterial occlusion. *J. Biomech.* 38, 647-655.
5. Kroll, M.H., Hellums, J. D., McIntire, L.V., Schafer,A.I., and Moake, J.L., (1996), Platelets and shear stress. *Blood Journal* 88(5): 1525-1541.
6. McDonald, D.A., (1960). *Blood Flow in Arteries* Williams & Wilkens, Baltimore.
7. Mynard, J.P. and Smolick, J. J. (2014), Wave potential and the one-dimensional wind kessel as a wave -based paradigm of diastolic arterial hemodynamics *Am J. Physiol. Heart Circ Physiol..* 307, H307-H318.

8. Nichols, W., O'Rouke, M., & Vlachopoulos, Ch. (2011), *McDonald's Blood Flow in Arteries: 6th Edition, Theoretical, Experimental and Clinical Principles*, CRC Press, Boca Raton.
9. Olsen, J. H., and Shapiro, A.H., (1967). Large-amplitude unsteady flow in liquid-filled elastic tubes, *J Fluid Mech.* 29, 513-538.
10. Parker, K.H., (2009), An brief history of arterial wave mechanics, *Med. Biol. Eng. Comput.* 47,111-118.
11. Parker, K.H., (2009), An introduction to wave intensity analysis, *Med. Biol. Eng. Comput.* 47,175-288.
12. Pedley, T.J.,(1980), *The Fluid Mechanics of Large Blood Vessels*, Cambridge Univ. Press.
13. Poirot, Maarten (2014),The Windkessel principle visualized. http://youtu.be/Bx9Nu2PkPsE.
14. Sadeghi, MR, Shirani, E., Tafazzoli-Shadpour, M, & Samaee,M. (2011), The effects of stenosis severity on the hemodynamic parameters-assessment of the correlation between stress phase angle and wall shear stress. *Journal of Biomech.* 44(15): 2614-2626
15. Samaee, M., Tafazzoli-Shadpour, M, & Alavi, (2017) Coupling of shear-circumferential stress pulses investigation through stress phase angle in FSI models of stenotic artery using experimental data. *Med. Biol. Eng. Comput.* 55, 1147-1162.
16. Stergiopulos, N., Meister, J.J. & Westerhop, N. (1999), Simple and accurate way for estimating total and segmental arterial compliance: the pulse pressure method. *Ann. Biomed. Eng.* 22, 393-397.
17. Tyberg, J. V., Shrive, N. G., Bouwmeester, J. C, . Parker, K. H, & Wang, J. Jr. (2010), The Reservoir-Wave Paradigm: Potential Implications for Hypertension, *Current Hypertension Reviews*, 4(3): 203-213.
18. Tyberg, J.V. Bouwmeester, J. C., Parker, K H., Shrive, N.G., & Wang, J.Jr. (2014), The case for the reservoir wave approach, *Int. J. Cardiology*, 172,299-306.
19. vandenBos, G. C., Westerhof, N., Elzinga,G., & Sipkema, P., (1976) Reflection in the systemic arterial system: effects of aortic and carotid occlusion. *Cardiovasc. Res.* 10, 565-573.
20. vandeVosse, F. N. & Sterogiulos, N., (2011), Pulse wave propagation in the arterial tree. *Annual Rev Fluid Mech.* 41: 467-499.
21. Westerhof, N. , Sipkema, P., van ven Bos, G. C., & Elzinga, G. (1972) Forward and backward waves in the arterial system. *Cardiovas. Res.* 6, 648-656.
22. Westerhof,N., Lankhaar, J-W. & Westerhopf, B.E.,(2009), The arterial Windkessel. *Med. Biolo. Eng.Comp.* , 47:131-141.
23. Wang, J.Jr. , O'Brien, A. B. , Shrive, N. G., Parker, K. H., & Tyberg, J.V. (2003), Time- domain representation of ventricular-arterial coupling as a windkessel and wave system,*Am J Physiol. Heart Circ. Physiol.* 284, H1358 -H1368.
24. Wang, J.Jr., Flewitt, J.A , Shrive, N. G., Parker, K. H., & Tyberg, J.V. (2006) Systemic venous circulation. Waves propagating on a windkessel: relation of arterial and venous windkessels to systemic vascular resistance. *Am J Physiol. Heart Circ. Physiol.* 284, H154 -H162.
25. Womersley, J.R., (1955), Oscillatory motion of a viscous fluid in a thin-walled elastic tube - The linear approximation for long waves. *Philo. Mag.* 46; 199-221.

Figures

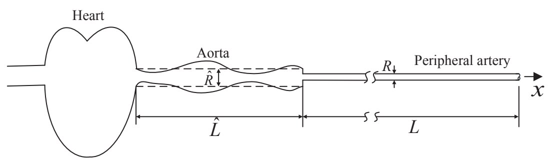

Fig. 1: Definition sketch of model vascular system

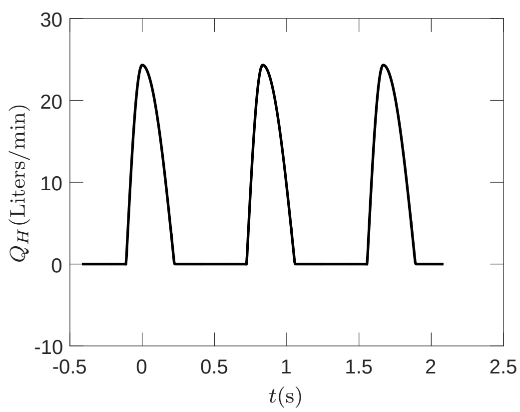

Fig. 2: A periodic series of influx pulses $Q_H(t)$ based on Eq. (2) for $a = 4T/15,\ b = 8T/15$. $U_{max} = 12.6\ cm/s$ Period of heart beat $2T$=0.834 (s).

.

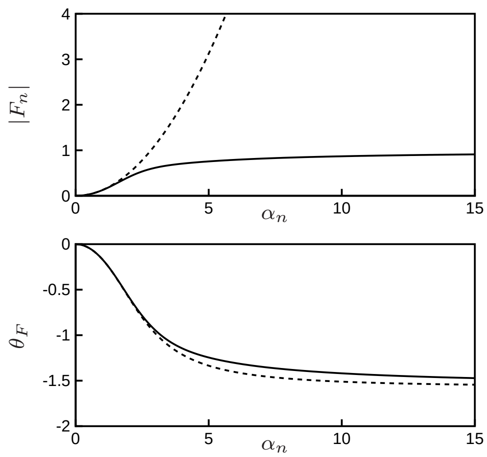

Fig. 3: Exact $F_n = |F_n|e^{i\theta_F}$ according to Eq.(43): (solid), and approximate F_n according to (Eq.48): (dashed), as functions of α_n

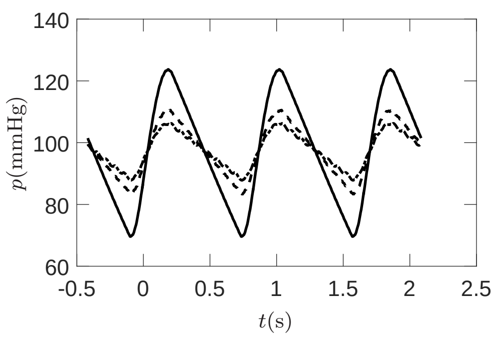

Fig. 4: Time variation of $p(\widehat{L}, t)$ at the junction $x = \widehat{L}$. Same aorta radius $\widehat{R} = 3\ cm$ but different lengths. Solid line: $\widehat{L} = 5\ cm$, Dashed line: $\widehat{L} = 10\ cm$, Dash-dot line: $\widehat{L} = 15\ cm$.

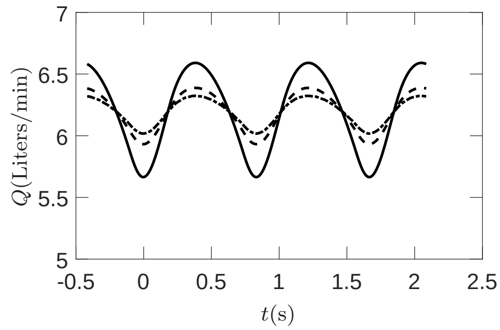

Fig. 5: Time variation of $Q(t)$ in peripheral artery. Same aorta radius $\widehat{R} = 3\ cm$ but different lengths. Solid line: $\widehat{L} = 5\ cm$, Dashed line: $\widehat{L} = 10\ cm$, Dash dot line: $\widehat{L} = 15\ cm$.

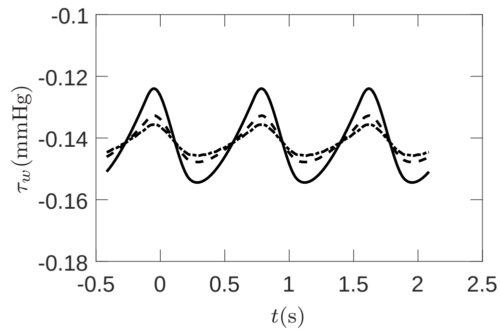

Fig. 6: Time variation of τ_w in peipheral artery. Same aorta radius $\widehat{R} = 3\ cm$ but different lengths. Solid line: $\widehat{L} = 5\ cm$, Dashed line: $\widehat{L} = 10\ cm$, Dash dot line: $\widehat{L} = 15\ cm$.

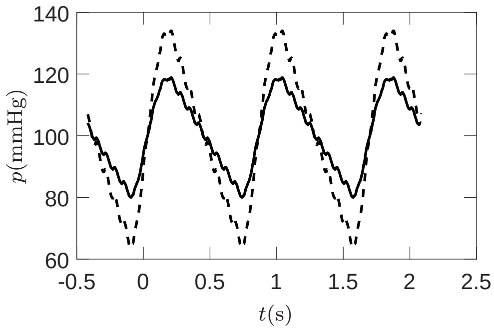

Fig. 7: Time variation of $p(\widehat{L},t)$ at the junction $x = \widehat{L}$. Same aorta length $\widehat{L} = 15$ cm but different radii. Solid line: $\widehat{R} = 2cm$, Dashed line: $\widehat{R} = 1.5cm$.

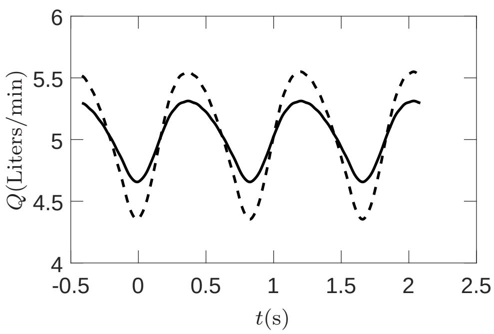

Fig. 8: Time variation of $Q(t)$ in peripheral artery. Same aorta length $\widehat{L} = 15$ cm but different radii. Solid line: $\widehat{R} = 2cm$, Dashed line: $\widehat{R} = 1.5cm$.

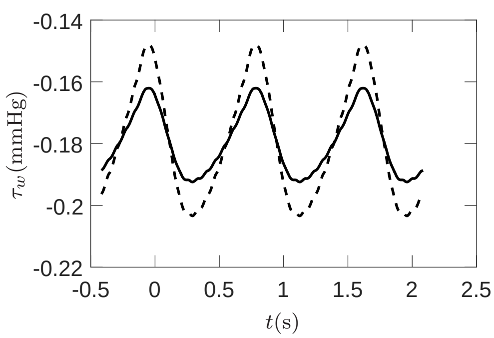

Fig. 9: Time variation of τ_w in peripheral artery. Same aorta length $\widehat{L} = 15$ cm but different radii. Solid line: $\widehat{R} = 2cm$, Dashed line: $\widehat{R} = 1.5cm$.